Eur. Phys. J. D **65**, 411–420 (2011)
DOI: 10.1140/epjd/e2011-20273-2

THE EUROPEAN PHYSICAL JOURNAL D

Regular Article

Structural evolution study of 1 −2 nm gold clusters

M.R. Beltrán[1,a], R. Suárez Raspopov[2], and G. González[1]

[1] Instituto de Investigaciones en Materiales, Universidad Nacional Aut´onoma de México, A.P. 70-360, C.P. 04510, Col. Copilco Universidad, México D.F., México
[2] Facultad de Ciencias, Universidad Nacional Aut´onoma de México, A.P. 04510, Col. Copilco Universidad, México D.F., México

Received 10 May 2011 / Received in final form 10 June 2011
Published online 22 November 2011 –

Abstract. We have explored lowest energy minima structures of gold atom clusters both, charged and neutral (Au_n^{ν} with $n = 20$, 28, 34, 38, 55, 75, 101, 146, 147, 192, 212 atoms and $\nu = 0, \pm 1$). The structures have been obtained from first principles generalized gradient approximation, density functional theory (DFT) calculations based on norm-conserving pseudopotentials and numerical atomic basis sets. We have found two new disordered or defective isomers lower in energy than their ordered counterparts for $n = 101$, 147. The purpose of this work is to systematically study the difference between the electronic properties of the two lowest ordered and disordered isomers for each size. Our results agree with previous first principle calculations and with some recent experimental results (Au_{20} and Au_{101}). For each case we report total energies, binding energies, ionization potentials, electron affinities, density of states, highest occupied molecular orbital-lowest unoccupied molecular orbital (HOMO-LUMO) gaps, Housdorff chirality measure index and their simulated image in a high resolution transmission electron microscopy (HRTEM). The calculated properties of the two low lying (ordered and disordered) isomers show clear differences as to be singled out in a suitable experimental setting. An extensive discussion on the evolution with size of the cohesive energy, the ionization potentials, the electron affinities, the HOMO-LUMO gaps and their index of chirality to determine the crossover between them is given.

1 Introduction

Applications of gold nanoclusters vary from bio-electronic devices [1,2], to building blocks for the creation of new nano-assembled materials that will be used to construct a new generation of devices such as organo-metallic nano circuits, nano sensors, nano catalytic agents, nano electronic machines (NEMS), etc. [3–10]. The quality of possessing different properties than their bulk counterparts, common to most cluster systems, seems particularly interesting amongst gold nanoclusters. For example, gold being a noble metal, becomes reactive, and even more non metallic properties have been observed at the nanoscale [11,12]. These new properties are size and structure geometry dependent. Therefore the precise knowledge of the cluster's structure, shape, morphology, surface, and chemical bonding is fundamental to be able to predict and understand their electronic, optical, and other properties. The determination of the cluster structures is still a challenge [13], which is evident from the existing ambiguity in the predictions for the geometry associated to gold nanoclusters between 1−2 nm in size. Important exceptions have recently been achieved for example Jadzinsky et al. [14] whom has reported the successful isolation, crystallization and structure determination by X-ray crystallography of a cluster with 102 gold atoms and 44 thiolates, corresponding to a truncated-decahedral cluster. Other relevant study on gold thiolate-protected Au_{38} has been performed by Lopez et al. [15]. And the systematic study performed by Chen et al. [16] on the Au_{16} following by both, theoretical and experimental results by Wang et al. [17], Bulusu et al. [18,19], and Xing et al. [20]. This area has produced a considerable amount of theoretical work, that has resulted in a large number and variety of structures, ranging from well known crystallographic forms [21–24], non crystallographic motifs [25], to disordered structures [26–28]. Nevertheless, both theoretical and experimental points of view reveal the truncated decahedral motif Mark's decahedra (M-Dh) as the predominantly leading structure around 1−3 nm [29–31]. Asencio et al., Cleveland et al. and Whetten et al. they all conclude that the Marks decahedra (M-Dh) motif is preferred from the Mackay icosahedra or the truncated octahedra sequence within the (1 −2) nm range. Other theoretical molecular dynamics studies done in the

[a] e-mail: mbeltran@unam.mx

1−100 nm range supporting this result have been carried out by Baletto [32] et al.

In this work, a density functional theory formalism based in the general gradient approximation (DFT-GGA) is used to explore lowest energy minima of Au_n^{ν} atom clusters for what is considered as magic numbers: $n = 20$, 28, 38, 55, 75, 101, 146, 147, 192, and 212, for charged as well as neutral systems ($\nu = 0, \pm 1$). Here, the concept of magic number is used in the purely geometrical sense, which is to have the precise number of atoms to build a highly geometrical structure such as a cuboctahedron, a decahedra, an icosahedra, etc. In this study we present two structures competing in energy for each size involved: one disordered, and one ordered. Our initial trial geometries are the result of a combination of techniques used in sequence. Starting out with global and unrestricted minimizations, by means of symbiotic genetic algorithms (SGA), and simulated quenching molecular dynamics (SQMD) [26,27,33,34]. From this initial study, which has been done for all structures here studied, the two lowest energy isomers are considered. One corresponding to a low energy ordered structure and another to the lowest disordered one, both of which are further fully minimized without symmetry constraints by means of local DFT-GGA method, based on norm-conserving pseudopotentials and numeric atomic basis sets [35–38] for every size here investigated. This procedure has been successfully used in earlier studies [28,39–41]. The purpose of this work is to analyze the electronic fingerprint of each isomer in detail, and to elucidate the possible different behavior of the disordered clusters due to symmetry reduction and to follow their evolution with size in order to estimate the crossover between ordered and disordered lowest energy structures. This study has been encouraged by previous theoretical and experimental results of Shaaff and Whetten [42], and Hakkinen et al. [43,44] pointing in this direction. A methodology based on the Hausdorff distance to quantify the degree of disorder has been used in this work[1] [45,46]. This method has emerged as the general method of choice for the quantification of chirality [14,40], and here it is referred as the index of chirality or Hausdorff chirality measure (HCM). This methodology is based solely on the geometry of the system, and it is independent of its chemical and physical manifestations. Our findings show that the lowest energy Au_n with $n = 28$, 34, 38, 55, 75, 101, 147 magic clusters correspond to disordered structures, while the most stable structures for Au_n for $n = 20$,146,192, and 212 correspond to the M-Dh family. We present total energies, binding energies, ionization potentials, electron affinities, density of states, HOMO-LUMO gaps, index of chirality, simulated HRTEM images and plots of their relative distances from the center of mass for each size.

Section 2 briefly describes the theoretical frame of this work. Section 3 presents our results, where we compare for the two lowest isomers, one ordered and one disordered, their relative total energies, their ionization potentials (IP), electron affinities (EA), binding energies (BE), HOMO-LUMO (H-L) gaps, index of chirality or (HCM), density of states (DOS), plots with the geometrical distribution of their atoms from the center of mass, and HRTEM images which show that defects in gold clusters of 1−2 nm can be resolved by this technique. The cluster size dependence of some properties will be discussed in this section, our results are compared with previous calculations and with experimental data when available. Section 4 presents our summary and final remarks.

2 Computational methods

Our initial approach to determine the lowest energy cluster configurations was based on global optimizations using simulated annealing (SA) and simulated quenching (SQ) techniques [47–49]. These are global optimization methods in which no assumptions are imposed on the cluster symmetry, in which fast cooling rates are applied to the system on selected regions of the phase space, where a catchment area of a local minimum is located. The n-body interaction modeling the metal cluster bonding is taken from the tight binding approximation to the second moment of the electronic density of states and are based on a genetic symbiotic evolutive algorithm [50]. This optimization method uses a Gupta n-body potential [34,51]. When this sequence of methods was applied, an interesting trend was observed: a set of nearly degenerate structures was obtained as the lowest lying isomers. Some of these structures could be classified as disordered. Some small clusters lack of planes of symmetry at all, while the larger ones present only local defects (mainly close to their surfaces). To quantify the degree of disorder we introduced a quantity called the chirality index, which we have used earlier [40] and will be described briefly here. In order to validate our findings we have performed a structure optimization analysis by means of density functional theory calculations, including self-consistent gradient corrections to the exchange-correlation energy. Scalar norm-conserving relativistic pseudopotentials in their fully non local form have been used [52,53], generated with the atomic valence electron configuration $5d^{10}6s^1$ and core radii (in units of a_0) for $s = 2.47$, $p = 2.98$, and $d = 2.00$ have been used [54], 11 electrons have been considered outside the core, unrestricted optimizations to the local stable energy minima have been performed. Perdew-Burke-Ernzerhof generalized gradient approximation (PBE-GGA) has been used for that effect [55]. A separate global minimization has been performed in each case for neutral and charged clusters. The relaxation criteria is considered to have been met once the maximum force component to an atom is less than 0.001 Hartree/a_0. For this purpose we have used the code SIESTA [35–37], where the basis functions and the

[1] The Hausdorff distance $h(Q, Q')$ between the sets Q and Q' can be defined as the smallest number $\delta = h(Q, Q')$ that has the following properties: (a) a spherical ball of radius δ centered at any point of Q contains at leat one point of Q' and (b) a spherical ball of radius δ centered at any point of Q' contains at least one point of Q. This definition was given in the two previous references.

electron density are projected onto a uniform real space grid in order to calculate the Hartree energy. The basis functions are considered as linear combinations of numerical (pseudo) atomic orbitals [56], allowing for double-ζ s, d basis and single-p polarization orbitals with a cut off radii of 6.72 Å. The grid fineness is controlled by means of an energy cutoff of the plane waves, the value (150 Ryd) has been used [37,56,57]. More computational details of the parameters and convergence tests for Au_2 and bulk gold have been previously described [39]. It is important to mention that spin polarization is not considered in this calculation. This methodology has been successfully used earlier [26–28,40,41,58–60], throwing results in agreement with high level correlation plane wave function calculations on very small clusters [61–63].

We have used an effective methodology to quantify the degree of disorder by means of the Hausdorff distance[1] [45,46], using the inherent structural symmetry of the clusters. Within this approach, the degree of chirality is found by calculating the maximum overlap between the actual molecular structure and its mirror image, using the Hasudorff distance between their sets of atomic coordinates[1]. By rotating and translating one structure with respect to the other, the optimal overlap can be calculated. This Hausdorff chirality measure (HCM) is a continuous and similarity invariant function of the molecular shape, and it is zero only if the molecule is achiral. The advantage of this approach is that its numerical implementation to the field of clusters is straightforward.

We calculate the HCM form the lowest energy structures using the relaxed cartesian coordinates measured with respect to the cluster center of mass. Through an inversion operation, the coordinates of the mirror image clusters were obtained. The HCM was obtained by calculating the maximum overlap between a given cluster and its mirror image. This corresponds to the minimum value of the Hausdorff distance between the sets of atomic coordinates of both structures. In order to obtain the minimum Hausdorff distance, the mirror cluster was translated and rotated by $\pi/360$ around the original cluster in the three dimensional space generating different configurations. For each of them, the Hausdorff distance with respect to the original cluster was calculated. The minimum of these values, normalized by the largest interatomic distance in the cluster, corresponds to the HCM. To further explore structural disorder in gold structures with size 1−2 nm, we have simulated HRTEM images using our lowest energy calculated cluster geometries and parameters corresponding to commercial microscope JEOL 2010 TEM. The Au clusters image simulation was made using SIMULATEM, [64] which is a software based on the multislice method of Cowley and Moodie [65]. This approximation is well adapted for this case because it can calculate images and diffraction patterns from arbitrary finite systems. Our presented HRTEM images were obtained based on the following microscope parameters: accelerating voltage = 200 keV, spherical aberration coefficient $Cs = 0.5$ nm, beam spread = 0.4 (mrad), defocus spread = 4 nm, Scherzer defocus = –35.4 nm. These optimal microscope conditions lead to a point to point resolution of 0.16 nm, which is enough to resolve the interatomic distance in gold clusters (0.24 nm in average), or in bulk gold (0.288 nm).

3 Results

We analyze the electronic properties of Au_n^{ν} with $n = 20$, 28, 34, 38, 55, 75, 101, 146, 147, 192, 212, for neutral as well as charged clusters ($\nu = 0, \pm 1$). First, we report two new disordered lowest energy configurations for $n = 101, 147$. This result may be added to the collection of disordered lowest energy structures previously reported both, theoretically as well as experimentally [26–28,40,41,43,44,58–60,66]. Figure 1 shows the equilibrium geometries for the lowest energy ordered or highly symmetric structures in the left hand side, and their simulated HRTEM images to their right. Similarly Figure 2 shows the lowest energy equilibrium geometries for disordered or lower symmetry isomers on the left columns, and their corresponding simulated HRTEM images to their right hand side. From these figures one can notice that for the larger clusters, the correspondence between the simulated HRTEM image and the projected structure when overlapped show a good point to point agreement. However, If the overlapping of atomic positions is weak, and the projected atomic distances are less than the instrumental resolution of 1.6 Å, then contrast differences appear between the simulated and the projected structures. This is the case for the Au_{28} both, T and disordered, the Au_{34} C1 and the Au_{55} disordered case. Nevertheless, contrast differences appear between ordered and disordered clusters as to be resolved experimentally, being more obvious the case for the larger ones.

In Figure 3 we show the atomic distances from the center of mass corresponding to the clusters shown in Figures 1 and 2. Here we can clearly observe the extent of the symmetry breaking inside the core of the disordered clusters (inverted triangles), where even the central atom for the smaller ones is affected, giving rise to an entirely different electronic fingerprint. While for the ordered structures (closed circles) the atomic layers are clearly differentiated. This type of study although simple in nature, could be an important tool to discern the local geometric configuration inside a metallic core. For completeness, a study of the atomic distances referred not to the center of mass, but to the innermost cluster atom has been performed to avoid spurious effects of not having a central atom in some cases. An although it is not shown here, both analysis are quite similar not presenting significant differences. Figure 4 shows the density of electronic states, obtained from the so called "Khon-Sham" eigenvalues for both, ordered and disordered isomers and for each size. For those cases where we can compare our results (for example the Au_{34} case), we agree well with the overall shape and H-L gaps as those published by Jalbout et al. [59,60,67]. From Figure 4 one can see that clear differences exist between the two isomers DOS near the Fermi level where the behavior of a material is primarily dictated. Table 1 resumes

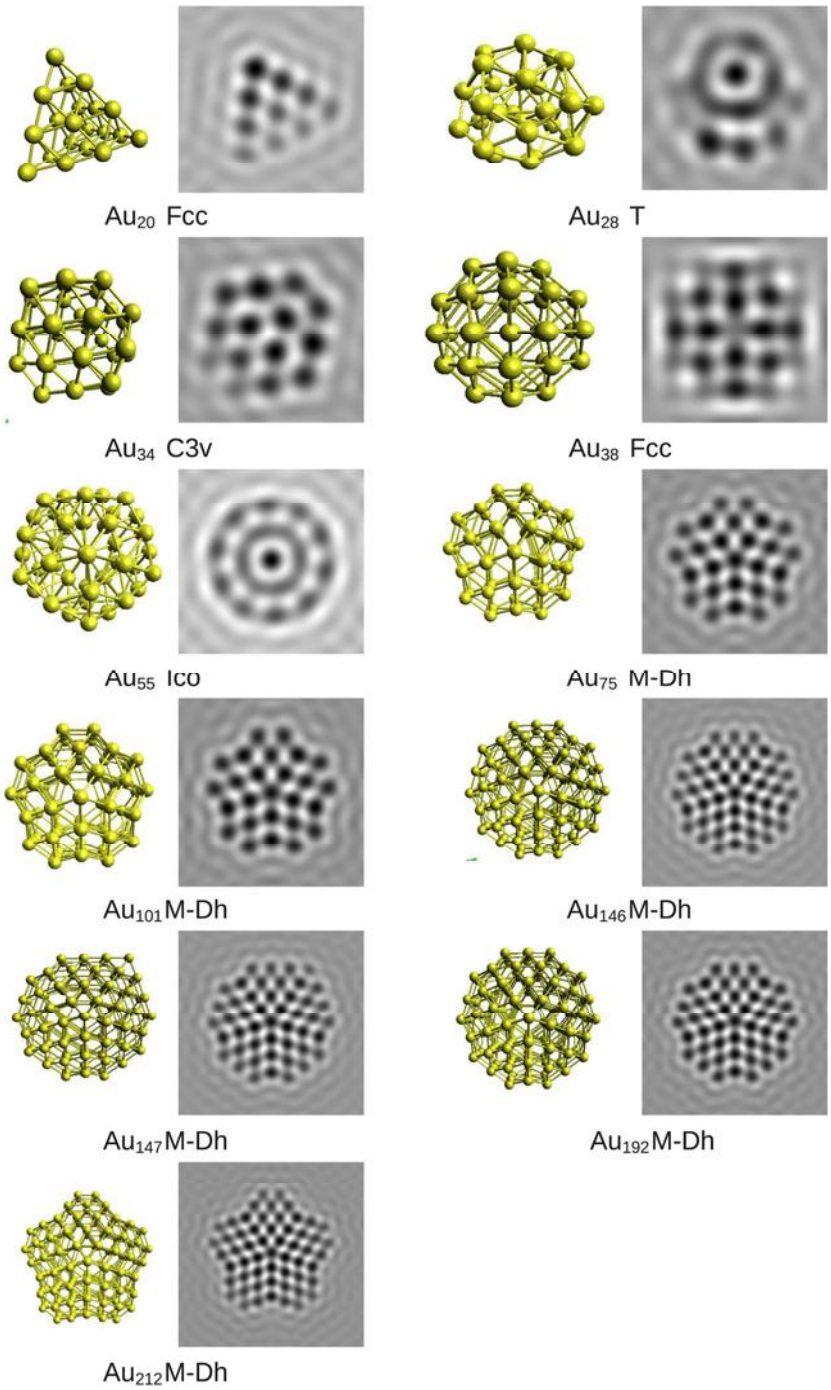

Fig. 1. (Color online) Atomic gold clusters for $n = 20$, 28, 34, 38, 55, 75, 101, 146, 147, 192, and 212 atoms. Highly symmetric structures are shown on the left hand columns and its corresponding calculated HRTEM images to their right.

the main features of the electronic behavior per pairs: ordered and disordered structures, and by size. Column 2 shows the relative energy difference between ordered and disordered structures. Notice that for some cases (Au_n n = 28, 34, 38, 55, 75, 101, 147) the disordered or low symmetry isomers have a lower energy. These results not only confirm our earlier findings where we have emphasized more relative stability towards low symmetry structures [26–28,40,41], but we found two new ones to be added to this sequence. The Au_{101} and the Au_{147} clusters, which to our knowledge have not been previously reported elsewhere. Column 3 shows the ionization potential $IP(Au_n) = E(Au_n^+) - E(Au_n^0)$. Notice that it decreases as a general trend as the cluster size increases, and in a non monotonically manner. It is important to observe that the ionization potential is slightly larger for the lowest energy minima in every case, except for Au_{28} cluster with T symmetry and for the Au_{75} ordered isomer. We will focus

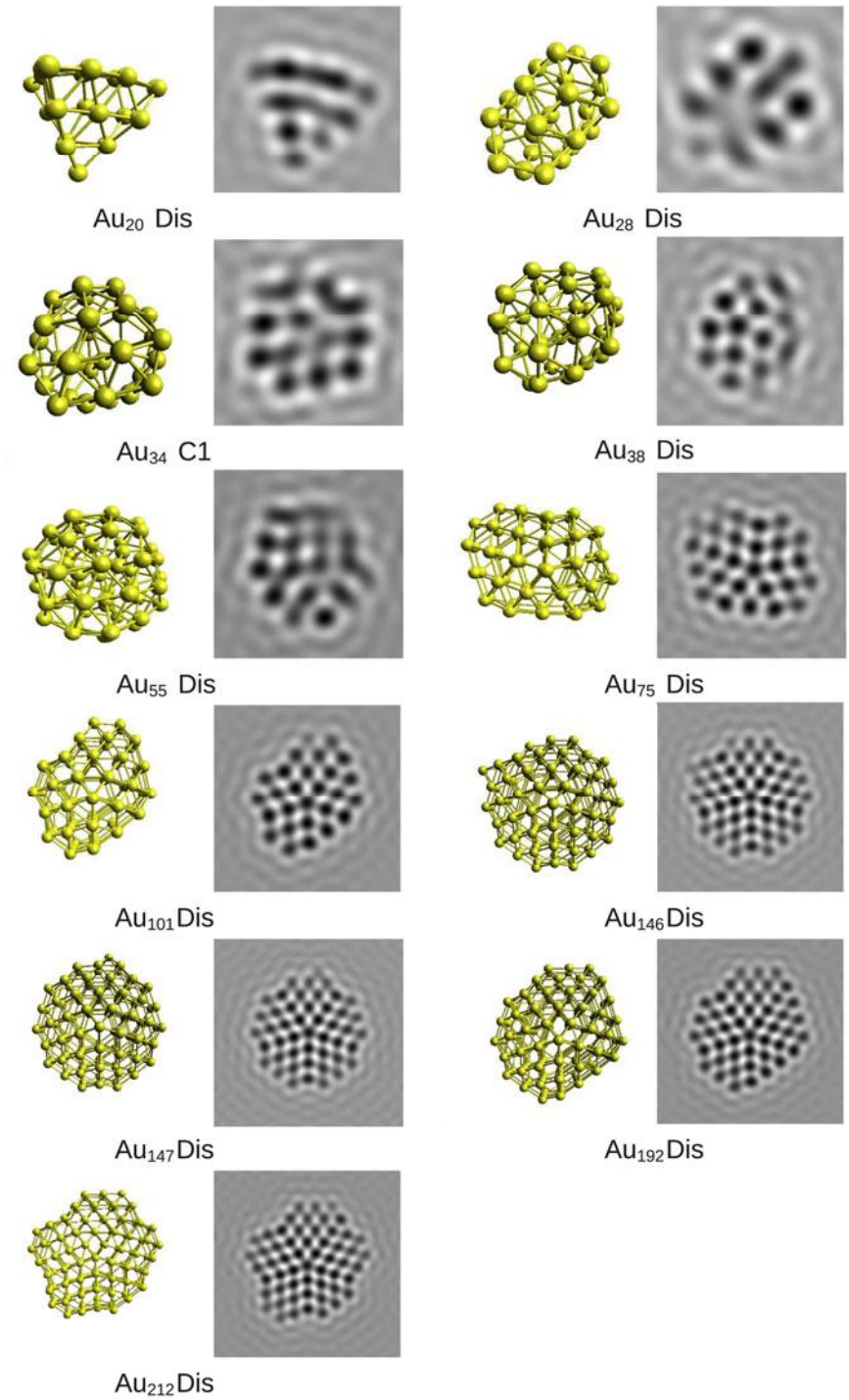

Fig. 2. (Color online) Atomic gold clusters for $n = 20$, 28, 34, 38, 55, 75, 101, 146, 147, 192, and 212 atoms. Disordered or low symmetry lowest energy isomers are shown on the left hand columns and their corresponding HRTEM images to their right.

our attention in the Au_{20} case as an important benchmark due to the fact that it has been extensively studied earlier [54,68–71]. Our ionization potential result of $IP = 6.456$ eV can be compared to the experimental value obtained by Jackschath et al. $IP = 7.82$ eV [69], as well as the result of Kryachko and Remacle [70], where two different values $IP = 7.398^a$ eV and $IP = 7.33^b$ eV are reported for: ^{a} B3LYP/LANL2DZ and ^{b} PW91/LANL2DZ relativistic pseudopotentials. Another example we can compare with, is the Au_{34} case which has been reported earlier by Gu et al. [24] with an $IP = 3.4$ eV for a C1 symmetry structure and $IP = 3.5$ eV for a C3v group structure. We also compare our result with an estimated value of $IP = 3.5$ eV obtained in the experiment reported

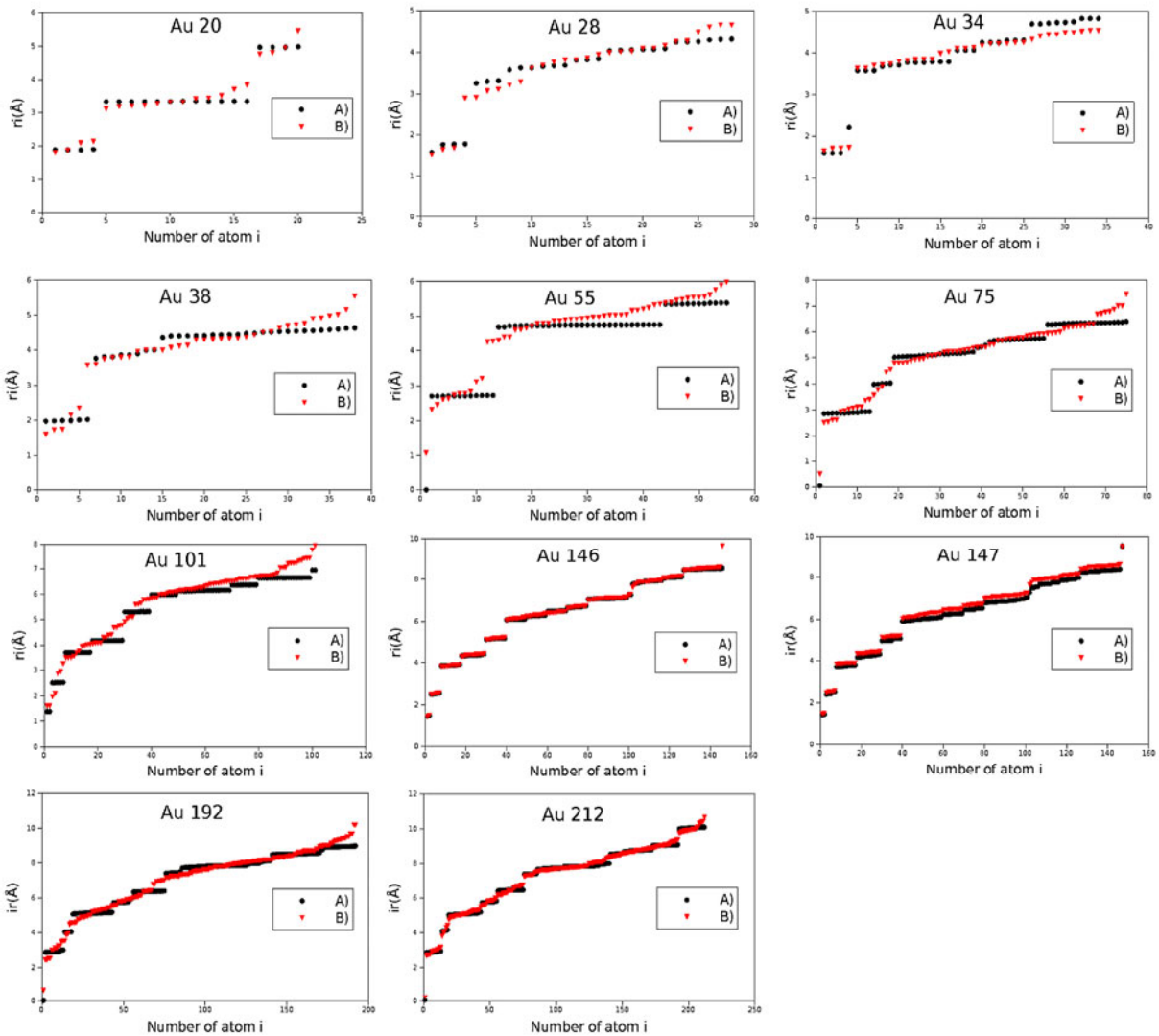

Fig. 3. (Color online) Atomic distance referred to the center of mass for Au_n, $n = 20$, 28, 34, 38, 55, 75, 101, 146, 147, 192, 212 atoms. Closed circles correspond to the atom positions for (A) ordered or high symmetry structures while the inverted triangles describe the disordered (B) or defective ones.

by Taylor et al. [72] Another interesting case is the Au_{55} cluster, where Periyasamy and Remacle report a calculated value of $IP = 6.36$ eV by means of relativistic B3LYP/LANL2MB [73].

In our Table 1 the fourth column shows the adiabatic electron affinity $AEA(Au_n) = E(Au_n^0) - E(Au_n^-)$. Notice that the adiabatic EA is given by the total energy difference between the neutral and the anionic cluster assuming that both structures have been fully relaxed separately. This quantity will be compared to the experimental (vertical) affinity, taken from measured vertical detachment energies (VDE's) of Au_n anions [72]. being therefore a lower bound for the experimental result. Furthermore, it is worth to mention that our calculated values for EA and IP are underestimated by the methodology used in this work, in a similar manner as the shell model, when compared with spin polarized small clusters [74]. Nevertheless, the values provided here, not only do not change considerably, but they also agree qualitatively well with the experimental values [72], for example for the Au_{20} case where the electron affinity experimental value is $EA = 2.732$ eV. In summary, the results of columns 3 and 4 in Table 1 emphasize a well known even-odd alternating behavior for both, IP and EA values earlier discussed in [75]. In which it is observed that in the even numbered clusters the electron affinities (EA's) is lower than in the odd numbered clusters. This may be explained because in the evenly neutral numbered clusters, the highest occupied molecular orbital (HOMO) is occupied by 2 electrons. While the odd-numbered neutral clusters (open shell species), have a hole in the HOMO. And the extra electron, which makes the cluster negative, occupy's either the LUMO of the even-numbered cluster, or the HOMO of the odd-numbered clusters. And as a result the EA's will be lower in the even atom clusters. Thus, the even-odd EA's and IP's oscillations reflects to some extent the spacing of the energy levels in the vicinity of the H-L gap. We observe that our values follow the correct

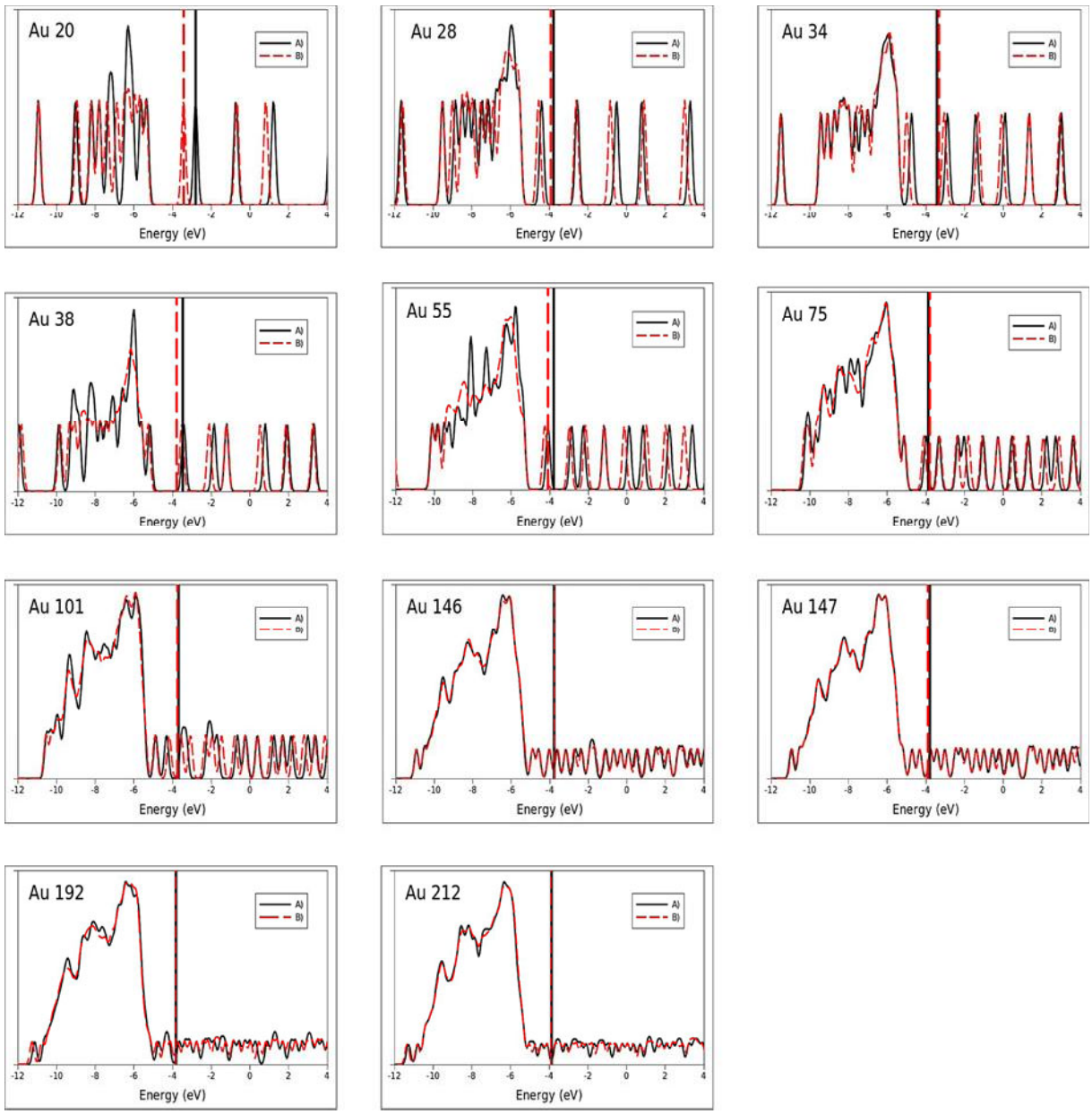

Fig. 4. (Color online) Density of states for the two lowest isomers for each size, $n = 20$, 34, 28, 38, 55, 75, 101, 146, 147, 192, 212 atoms, (A) corresponds to the high symmetry structure s and (B) to the disordered lowest minima as in Figures 1 and 2. The tall vertical dark line in each graph, represents the Femi level.

trend towards the bulk work function $WF = 5.1$ eV. Also, notice that as the size of the cluster increases in Table 1 for example for $n = 146$, 147, and 212 the odd-even behavior in both IP and EA becomes much less important. This happens as the density of the electronic states increases with the cluster size particularly around the HOMO. This effect can be clearly followed along the DOS of the different cluster sizes in Figure 4. This HOMO energy states congestion represents the initial stage of a smooth transition to a metallic state.

The fifth column in Table 1 shows the binding energy per atom. Our calculated bench mark BE for the Au_{20} fcc is 3.207 eV, similar to Fernandez et al. [54] value $BE = 3.17$ eV as essentially the same methodology has been used. The binding energi es increase non monotonically with the cluster size as ex pected. Columns six, seven and eight in Table 1 show the HOMO-LUMO (H-L) gap for anions, cations and neutral species. One can first notice that the electronic behavior of the charged species is not necessarily the same as the neutrals, for example in the case of Au_{55} the H-L is one order of magnitude larger for the anionic case. This has also been highlighted in previous studies [59,60,68]. The H-L gap opens up considerably for Au_n $n = 20, 34$, where non-metallic behavior is expected to be observed, but the H-L gaps closes up as the cluster size increases and a metallic behavior takes

Table 1. Optimized low-lying structures for two Au_n one ordered and one disordered for $n = \{20, 34, 28, 38, 55, 75, 101, 146, 147, 192, 212\}$ atoms. The relative total energy (ΔE), the ionization potential (IP), the electronic affinity (EA), the binding energy per atom (BE), the HOMO-LUMO gaps (H-L$^{\nu}$), where $\nu = 0, \pm 1$, and finally the Hausdorff chirality measure (HCM) are shown.

Cluster	ΔE (eV)	IP (eV)	EA (eV)	BE (eV)	H-L^0 (eV)	H-L^1 (eV)	H-L^{-1} (eV)	HCM
Au_{20} Fcc	0.000	6.456	1.127	3.207	1.856	1.999	1.791	0.00
Au_{20} Dis	1.355	6.102	1.997	3.139	1.128	1.081	0.912	0.13
Au_{28} T	0.185	5.929	2.533	3.239	0.360	0.305	0.335	0.15
Au_{28} Dis	0.000	5.600	2.617	3.246	0.296	0.249	0.132	0.11
Au_{34} C3	0.159	5.877	1.963	3.387	0.942	0.905	0.861	0.12
Au_{34} C1	0.000	5.845	1.911	3.392	1.069	1.018	0.996	0.11
Au_{38} Fcc	0.905	4.811	2.201	3.360	0.043	0.023	0.053	0.00
Au_{38} Dis	0.000	5.015	2.503	3.384	0.106	0.083	0.061	0.02
Au_{55} Ico	0.390	5.164	3.016	3.500	0.205	0.114	0.608	0.00
Au_{55} Dis	0.000	5.196	2.945	3.507	0.069	0.036	0.134	0.11
Au_{75} M-Dh	0.567	5.002	2.845	3.572	0.034	0.004	0.055	0.00
Au_{75} Dis	0.000	4.931	2.873	3.580	0.074	0.015	0.147	0.01
Au_{101} M-Dh	0.149	4.715	2.720	3.639	0.036	0.009	0.057	0.00
Au_{101} Dis	0.000	4.813	2.836	3.640	0.084	0.067	0.092	0.10
Au_{146} M-Dh	0.000	4.682	2.908	3.729	0.013	0.012	0.034	0.00
Au_{146} Dis	0.181	4.835	2.888	3.728	0.168	0.174	0.147	0.10
Au_{147} M-Dh	0.313	4.665	2.906	3.728	0.029	0.019	0.034	0.00
Au_{147} Dis	0.000	4.682	2.913	3.730	0.025	0.019	0.027	0.01
Au_{192} M-Dh	0.000	4.684	2.886	3.778	0.032	0.026	0.012	0.00
Au_{192} Dis	1.421	4.728	2.999	3.771	0.067	0.067	0.066	0.01
Au_{212} M-Dh	0.000	4.675	3.077	3.792	0.009	0.003	0.010	0.00
Au_{212} Dis	0.312	4.715	3.019	3.791	0.082	0.062	0.075	0.07

place above Au_{75}. In the same way as the cluster size increases, the energy gap between ordered versus disordered structures, decreases. But as expected in a critical size zone, it behaves non monotonically. Our H-L gap for Au_{20} H-L = 1.85 eV is to be compared to H-L = 1.77 eV [73], and H-L = 1.83 eV reported by Fernandez et al. [54] actually discussed for the first time by Li et al. [68]. We compare with Au_{34}, where several theoretical studies have predicted HOMO-LUMO gaps for the C1 and C3v structures with values: H-L = 0.99 eV and H-L = 0.58 eV respectively [59,60]. This compares well with our result for C1 H-L = 1.06 eV, while not so good for C3v for which we obtain H-L = 0.94 eV surely due to structural differences that can be seen from its corresponding graph shown in Figure 3. The last column (column 9) in Table 1 reports the Hausdorff chirality measure (HCM). From its definition this quantity takes a value within zero, for symmetric structures to a maximum of 1, for disordered or low symmetry ones. This quantity represents a measure of the degree of disorder and it is easy to understand its meaning with the geometrical analysis discussed and shown in Figures 1, 2 and 3. Notice that if the structure have well defined planes and overall symmetry it makes them achiral and have an HCM of zero (such is the case for $Au_{20,38}$ fcc, Au_{55} ico, and $Au_{75,101,146,147,192,212}$ M-Dh), while disordered clusters either lack of symmetry planes or have local defects, being chiral in nature. For the latter the HCM index is the highest for Au_{28} disordered structure, as it shows no symmetry at all, followed by our also highly asymmetric Au_{20} disordered cluster, but one notices how the HCM diminishes as the cluster size increases. This is clearly a reflect that the larger the cluster the less defects they present, the larger ones (Au_{146} and up) having only local point defects that are located close to the surface. This findings could be confirmed by means of circular dichroism experiments on which we actually sustain our result for the Au_{28} and Au_{38} in which optical activity has been reported by Shaaff and Whetten [42], and has been discussed in an earlier publication [40]. We report the findings of two new disorder low energy structures: $Au_{101,147}$. The first structure Au_{101} is disordered from the very core of its structure as can be clearly seen in Figure 3. This structure is 0.1 eV more stable than its symmetric counterpart, and this is reflected through its electronic properties. It presents a metallic behavior in its H-L gap, as can be seen from Table 1 in columns 6−8. Au_{147} has only a localized defect near its surface (see HRTEM image in Figs. 1 and 2). Despite this fact , its relative energy versus the more symmetric Au_{147} M-Dh counterpart differs by 0.313 eV, but this energy difference is not so clearly reflected in the rest of its electronic properties as more dominant bulk characteristics start to set in. We finally remark that our equilibrium geometries for Au_n, for $n = 20, 34, 55$ are in overall agreement with recent calculations [67,70,73,76], as well as with the available experimental data [43,44,68].

4 Summary

We present a systematic study of the electronic properties and the geometric structure of gold clusters Au_n^{ν}; $\nu = 0, \pm 1$ obtained from first principles GGA density functional calculations based in norm-conserving

pseudopotentials, and numerical atomic basis sets. We obtain the ground state energy configurations of the anionic, neutral and cationic gold clusters for two cases, one a highly symmetric cluster and another for a low symmetry or disordered structure, for sizes corresponding to $n = 20$, 34, 28, 38, 55, 75, 101, 146, 147, 192, and 212 atoms respectively. These non spin polarized results are the only systematic prediction for the geometries of gold clusters in this size range to our knowledge, and we may emphasize that they depend only on the accuracy of our numerical constraints, and on our initial geometry global search.

Our results agree in general with experimental photoelectron spectral data [43,44,72], as well as with recent experimental findings [14,68], for some cluster sizes and with previous theoretical calculations [24,59,60,67,69,70,73,77]. A new set of disordered or low symmetry configurations was found to be the most stable (101, 147 gold atom cases), which have not been reported earlier. Nevertheless fcc and icosahedral structures where also found as local minima of the PES competing close in energy. This results where obtained through global optimization methods followed by first principle calculation (DFT-GGA). In overall we have explored the plausibility that low symmetry disordered isomers may have higher energetic stability than ordered ones. As for the physical properties here studied, we observe and discuss extensively trends for the cohesive energy, ionization potentials, electron affinities, HRTEM images, their chirality in terms of the Hausdorff distance and HOMO-LUMO gaps, as the cluster size increases, and as the charge state changes. Additional effort is necessary for the calculation and classification of the physical properties of larger most stable isomers that characterize the potential energy surface of gold cluster. Work in such direction is currently in progress as well as the roll of surface passivation and deposition on a given surface and its interaction with it.

References

1. N. Lidgi-Guigui, C. Leung, R.E. Palmer, Surf. Sci. **602**, 1006 (2008)
2. R.E. Palmer, C. Leung, Trends Biotechnol. **25**, 48 (2006)
3. R.P. Andres, T. Bein, M. Dorogi, S. Feng, J.I. Henderson, C.P. Kubiak, W. Mahoney, R.G. Osifchin, R. Reiefenberger, Science **272**, 1323 (1996)
4. R.P. Andres, J.D. Bielefeld, J.I. Henderson, D.B. Janes, V.R. Kolagunta, C.P. Kubiak, W.J. Mahoney, R.G. Osifchin, Science **273**, 1690 (1996)
5. P. Alivisatos, K.P. Johnsson, X. Peng, T.E. Wilson, C.J. Loweth, M.P. Bruchez, P.G. Schultz, Nature **382**, 609 (1996)
6. A.P. Alivisatos, Science **271**, 933 (1996)
7. P. Alivisatos, Nat. Biotechnol. **22**, 47 (2004)
8. M. Haruta, Catal. Today **36**, 153 (1997)
9. R.J.C. Batista, H. Chacham, M.S.C. Mazzoni, I.L. Garzón, M.R. Beltrán, Phys. Rev. Lett. **96**, 116802 (2006)
10. R.J.C. Batista, P. Ordejón, H. Chacham, E. Artacho, Phys. Rev. B **75**, 041402 (2007)
11. A. Sanchez, S. Abbet, U. Heiz, W.D. Schneider, H. Häkkinen, R.N. Barnett, U. Landman. J. Phys. Chem. A **103**, 9573 (1999)
12. T.P. Martin, Phys. Rev. **273**, 199 (1993)
13. S.J.L. Billinge, I. Levin, Science **316**, 561 (2007)
14. P.D. Jadzinsky, G. Calero, C.J. Ackerson, D.A. Bushnell, R.D. Kornberg, Science **318**, 430 (2007)
15. O. Lopez-Acevedo, H. Tsunoyama, T. Tsukuda, H. Häkkinen, C.M. Aikens, J. Am. Chem. Soc. **132**, 8210 (2010)
16. G. Chen, Q. Wang, Q. Sun, Y. Kawazoe, P. Jena, J. Chem. Phys. **132**, 194306 (2010)
17. J. Wang, G. Wang, J. Zhao, Phys. Rev. B **66**, 035418 (2002)
18. S. Bulusu, X. Li, S. Wang, X.C. Zeng, Porc. Natl. Acad. Sci. USA **103**, 8326 (2006)
19. S. Bulusu, X.C. Zeng, J. Chem. Phys. **125**, 154303 (2006)
20. X. Xing, B. Yoon, U. Landman, J.H. Parks, Phys. Rev. B **74**, 165423 (2006)
21. J.P.K. Doye, D.J. Wales, Phys. Rev. Lett. **80**, 1357 (1998)
22. J.P.K. Doye, D.J. Wales, Phys. Rev. Lett. **86**, 5719 (2001)
23. D.J. Wales, *Energy Landscapes with Applications to Clusters, Biomolecules and Glasses* (Cambridge University Press, Cambridge, 2003)
24. X. Gu, M. Ji, S.H. Wei, X.G. Gong, Phys. Rev. B **70**, 205401 (2004)
25. O.D. Haberlen, S.C. Chung, N. Rosch, Ber. Bunsen-Ges. Phys. Chem. **98**, 882 (1994)
26. I.L. Garzón, K. Michaelian, M.R. Beltrán, A. Posada-Amarillas, P. Ordejón, E. Artacho, D. Sánchez Portal, J. Soler, Phys. Rev. Lett. **81**, 1600 (1998)
27. I.L. Garzón, A. Posada-Amarillas, Phys. Rev. B **54**, 11796 (1996)
28. I.L. Garzón, K. Michaelian, M.R. Beltrán, A. Posada-Amarillas, P. Ordejón, E. Artacho, D. Sánchez Portal, J. Soler, Eur. Phys. J. D **9**, 211 (1999)
29. J.A. Ascencio, C. Gutiérrez-Wing, M.E. Espinosa, M. Marín, S. Tehuacanero, C. Zorrilla, M. José-Yacamán, Surf. Sci. **396**, 349 (1998)
30. C.L. Cleveland, U. Landman, T.G. Schaaff, M.N. Shafigullin, P.W. Stephens, R.L. Whetten, Phys. Rev. Lett. **79**, 1873 (1997)
31. R.L. Whetten, J.T. Khoury, M.M. Alvarez, S. Murthy, I. Vezmar, Z.L. Wang, P.W. Stephens, C.L. Cleveland, W.D. Luedtke, U. Landman, Adv. Mat. **8**, 428 (1996)
32. F. Baletto, R. Ferrando, A. Fortunelli, F. Montalenti, C. Mottet, J. Chem. Phys. **116**, 3856 (2002)
33. K. Michaelian, N. Rendón, I.L. Garzón, Phys. Rev. B **60**, 2000 (1999)
34. R.P. Gupta, Phys. Rev. B **23**, 6265 (1981)
35. P. Ordejón, E. Artacho, J.M. Soler, Phys. Rev. B **53**, 10 441 (1996)
36. D. Sánchez-Portal, P. Ordejón, E. Artacho, J.M. Soler, Int. J. Quantum Chem. **65**, 453 (1997)
37. E. Artacho, D. Sánchez-Portal, P. Ordejón, A. García, J.M. Soler, Phys. Status Solidi B **215**, 809 (1999)
38. W. Khon, L.J. Sham, Phys. Rev. **140**, 1133 (1965)
39. J.M. Soler, M.R. Beltrán, K. Michaelian, I.L. Garzon, P. Ordejón, D. Sanchez-Portal, E. Artacho, Phys. Rev. B **61**, 5771 (2000)
40. I.L. Garzón, J.A. Reyes, J.I.L. Rodríguez Hernámdez, I. Sigal, M.R. Beltrán, K. Michaelian, Phys. Rev. B **66**, 073403 (2002)
41. I.L. Garzón, E. Artacho, M.R. Beltrán, A. García, J. Junquera, K. Michaelian, P. Ordejón, D. Sánchez-Portal, J.M. Soler, Nanotechnology **12**, 126 (2001)

42. T.G. Schaaff, R.L. Whetten. J. Phys. Chem. B **104**, 2630 (2000)
43. H. Häkkinen, M. Moseler, O. Kostko, N. Morgner, M. Astruc Hoffmann, B.V. Issendorff, Phys. Rev. Lett. **93**, 093401 (2004)
44. H. Häkkinen, M. Walter, H. Grönbeck, J. Phys. Chem. B **110**, 9927 (2006)
45. A.B. Buda, K. Mislow, J. Am. Chem. Soc. **114**, 6006 (1992)
46. A.B. Buda, T. Auf def Heyde, K. Mislow, Angew. Chem. Int. Ed. Engl. **31**, 989 (1992)
47. J. Jellinek, I.L. Garzón, Z. Phys. D **20**, 239 (1991)
48. I.L. Garzón, J. Jellinek, Z. Phys. D **20**, 235 (1991)
49. I.L. Garzón, J. Jellinek, Z. Phys. D **26**, 316 (1993)
50. K. Michaelian, Am. J. Phys. **66**, 231 (1998)
51. V. Rossato, M. Guillope, B. Legrand, Philos. Mag. A **59**, 321 (1989)
52. N. Troullier, J.L. Martins, Phys. Rev. B **43**, 1993 (1991)
53. L. Kleinman, D.M. Bylander, Phys. Rev. Lett. **48**, 1425 (1982)
54. E.M. Fernández, J.M. Soler, I.L. Garzón, L.C. Balbás, Phys. Rev. B **70**, 165403 (2004)
55. J.P. Perdew, K. Burke, M. Ernzerhof, Phys. Rev. B **77**, 3865 (1996)
56. O.F. Sankey, D.J. Niklewski, Phys. Rev. B **40**, 3979 (1989)
57. W.H. Press, S.A. Teukolsky, W.T. Vetterling, B.P. Flannery, *Numerical Recipes. The Art of Scientific Computing* (Cambridge University Press, Cambridge, 1992)
58. J.M. Soler, M.R. Beltrán, K. Michaelian, I.L. Garzón, P. Ordejón, D. Sánchez Portal, E. Artacho, Phys. Rev. B **61**, 5771 (2000)
59. A.F. Jalbout, F.F. Contreras-Torres, L.A. Pérez, I.L. Garzón, J. Phys. Chem. A **112**, 353 (2008)
60. I.E. Santizo, F. Hidalgo, L.A. Pérez, C. Noguez, I.L. Garzón, J. Phys. Chem. C **112**, 17533 (2008)
61. R.M. Olson, M.S. Gordon, J. Chem. Phys. **126**, 214310 (2007)
62. R.M. Olson, S. Varganov, M.S. Gordon, H. Metiu, S. Chretien, P. Piecuch, K. Kowalski, S. Kucharski, M. Musial, J. Am. Chem. Soc. **127**, 1049 (2005)
63. I.L. Garzón, C. Rovira, K. Michaelian, M.R. Beltrán, P. Ordejón, J. Junquera, D. Sanchez-Portal, E. Artacho, J.M. Soler, Phys. Rev. Lett. **85**, 5250 (2000)
64. A. Gómes Rodríguez, L.M. Beltrán del Rio, R. Herrera Becerra, Ultramicroscopy **110**, 95 (2010)
65. J.M. Cowley, A.F. Moodie, Acta Cryst. **10**, 609 (1957)
66. R.L. Whetten, R.C. Price, Science **318**, 407 (2007)
67. X. Gu, S. Bulusu, X. Li, X.C. Zeng, J. Li, X.G. Gong, L.S. Wang, J. Phys. Chem. C **111**, 8228 (2007)
68. J. Li, X. Li, H.J. Zhai, L.S. Wang, Science **299**, 864 (2003)
69. C. Jackschath, I. Rabin, W. Ber Bunsenges Schulz, Phys. Chem. **86**, 1200 (1992)
70. E.S. Kryachko, F. Remacle, Int. J. Quantum Chem. **107**, 2922 (2007)
71. X. Xing, B. Yoon, U. Landman, J.H. Parks, Phys. Rev. B **74**, 165423 (2006)
72. K.J. Taylor, C.L. Pettiette-Hall, O. Cheshnovsky, R.E. Smalley, J. Chem. Phys. **96**, 3319 (1992)
73. G. Periyasami, F. Remacle, Nano Lett. **9**, 3007 (2009)
74. P. Pyykkö, Chem. Soc. Rev. **37**, 1967 (2008)
75. S.T. Arnold, J.G. Eaton, D. Patel-Misra, H.W. Sarkas, K.H. Bowen, *Ion and Cluster Ion Spectroscopy and Structure* (Elsevier, Amsterdam, 1988), p. 147
76. J. Wang, G. Wang, J. Zhao, Chem. Phys. Lett. **380**, 716 (2003)
77. V.A. Spasov, Y. Shi, K.M. Ervin, Chem. Phys. **262**, 75 (2000)